Article

Adaptive Dynamic Building Envelopes with Solar Power Components: Annual Performance Assessment for Two Pilot Sites

Renos Rotas [1,2] , Maria Fotopoulou [1] , Panagiotis Drosatos [1] , Dimitrios Rakopoulos [1,*] and Nikos Nikolopoulos [1]

1   Centre for Research and Technology Hellas, Chemical Process and Energy Resources Institute, 52 Egialias Str., 15125 Athens, Greece
2   Laboratory of Applied Thermodynamics, Department of Mechanical Engineering, Aristotle University of Thessaloniki, 54124 Thessaloniki, Greece
*   Correspondence: rakopoulos@certh.gr; Tel.: +30-210-6899-689

Abstract: Energy consumption reduction and thermal quality improvement constitute two major aspects of building design and/or retrofitting. Following the current energy transition trends, a state-of-the-art solution is the implementation of Adaptive Dynamic Building Envelopes (ADBEs), which are capable of integrating different technologies and components. The purpose of this investigation is to assess the annual performance improvement of two actual building spaces retrofitted with ADBEs, consisting of Building Integrated Photovoltaics (BIPVs), additional thermal insulation, mechanical ventilation system with heat recovery, and solar air heaters (SAHs). Both buildings are pilot sites for the EU Horizon 2020 Plug-n-Harvest project and are located in two rather different climate zones, i.e., Cardiff, Wales, and Grevena, Greece. Moreover, through detailed dynamic modeling with the use of Modelica language, this study attempts to accurately capture all interactions between buildings and all the aforementioned ADBE components. The simulations compared the energy performance and indoor temperature levels in each space before and after the installation of the ADBEs. The results showed that the harvesting of renewable energy through the ADBE system could potentially contribute 60% and 21.8% to the annual electricity and heating load of the space in Cardiff, respectively, and 43.5% to the annual electricity load of the building space in Grevena.

Keywords: adaptive dynamic building envelope; building integrated photovoltaic; building energy performance simulation; energy consumption; solar air heater

1. Introduction

Energy demand increase and its negative impact on the environment is a major issue with economic and social dimensions. The building sector represents 30% of global final energy consumption and 27% of total energy sector emissions [1,2]. In this context, the architecture of buildings is being revised to promote performance enhancement, energy loss reduction, and even contribution to energy production [3].

Regarding the retrofitting of a building for status improvement, the most common practices are conventional retrofitting, implementation of Building Automation Systems (BASs), and use of advanced Adaptive Dynamic Building Envelopes (ADBEs) [3–5]. Conventional retrofitting is the simplest approach towards the improvement of the building and suggests the enhancement or replacement of the existing construction with more efficient, passive components and materials [4]. This may result in energy consumption reduction at the expense of high installation costs. In addition, conventional retrofitting is a passive way to improve the building envelope and does not provide the possibility for self-consumption through Renewable Energy Sources (RES). On the other hand, BASs include technologies, such as sensors and communication systems, which are capable of harvesting energy from

RES with demand response and demand shaping attributes provided that a form of RES is already installed in the building [5]. Nevertheless, this solution is less effective at reducing energy consumption compared to conventional retrofitting. Finally, the concept of ADBEs suggests the combination of active and passive modules on the building envelope and contributes towards loss reduction, and improvement of thermal quality, RES generation, and self-consumption [6]. In this way, ADBE systems result in significant energy consumption reduction and RES harvesting, which renders them the most effective option.

Technologies that have emerged as possible components for ADBE systems include solar power modules, Phase Change Materials (PCMs), insulation, algae bioreactor façade systems, etc. [7,8]. Out of all these options, solar power modules have gained much attention over the past few years, due to certain unique advantages over their alternatives. This category includes renewable energy production through photovoltaic (PV) systems, mostly Building Integrated PVs (BIPVs) [9], which enhance the self-consumption capability and the environmentally friendly behavior of the buildings [10]. Furthermore, BIPVs are capable of incorporating additional components, such as Solar Air Heaters (SAHs) and Photovoltaic–Thermal (PVT) collectors, to recover solar radiation either directly or through the heated air behind the panels. In both cases, mechanical ventilation systems are already installed or can be incorporated to drive the heated air into the interior for heating and ventilation [11].

Due to the significance of the above technologies in the context of the ongoing energy transition of buildings, several researchers have approached this field of development over the past few years. For example, Calise et al. [12] used TRNSYS [13] to study the potential energy and financial benefits from the combination of roof-mounted BIPVs, small-scale Wind Turbines (WTs), and heat pumps for the multigeneration of heating, cooling, electricity, and domestic hot water (DHW) in a hotel. According to the results, renewable electricity generation could cover 61% of the hotel's annual electricity demand and the heat pump adoption could lead to a reduction of the primary energy demand by 27% for heating, cooling, and DHW purposes. Moreover, Kant et al. [14] studied the behavior of a façade combining a PCM unit attached at the back surface of Building-Integrated Photovoltaic/Thermal (BIPV/T) panels, and a ventilated air gap between the components and the existing wall. More specifically, the study simulated the BIPV/PCM temperature spatial distribution using COMSOL Multiphysics [15]. Moreover, in the framework of a design optimization procedure, the effect of various parameters, such as the PCM material type and thickness, the BIPV height, and the air channel thickness, on the PV electricity generation and the energy extracted by the air ventilation system has been examined. The selection of the proper characteristics is able to increase the total energy extraction by approximately 650%, proving the significance of such components to the energy efficiency improvement of the buildings. Yet, the analysis focused on the integrated façade itself, neglecting interactions with building thermal zones. In Ref. [16], the cooling potential of a desiccant cooling machine in the Mataró library building (Spain) was studied, when the latter was supplied by ventilated PV/SAH units mounted on façades. According to the results of the simulations conducted in TRNSYS, on average, 93% of the cooling demand during the summer could be covered by the solar-powered system. Furthermore, Yang et al. [17] assessed the energy performance of various topologies of Double-Skin Façades (DSFs) in three Australian climate zones. In this context, numerical simulations in TRNSYS evaluated the energy consumption of a 5.6 m^2 single-zone building, when the façade was equipped with non-ventilated BIPV, naturally ventilated BIPV/T or mechanically ventilated BIPV/T systems. According to the results, a total annual energy savings of 34.1%, 86%, and 106% could be attained with the optimal configuration in Darwin, Sydney, and Canberra, respectively. Additionally, Alhammadi et al. [18] presented the testing and validation of façades with naturally ventilated BIPVs in desert climates. According to the results, the annual energy yield of the south modules was higher than the east and west modules, making it an optimal orientation for BIPV façades. Yet, the east and west façades could produce up to 40.9% more energy than the south from April to August, which are months with high energy demand in countries with hot climates. In a slightly different

and more modern approach, Nguyen et al. [19] developed an Artificial Neural Network (ANN) to exclusively predict the annual output energy of a BIPV system, using one-month datasets of spectral and environmental databases of Gifu, Japan. Based on the results, the annual efficiency of the system could range from 7% to 23%, depending on its orientation.

Based on this literature review, it is evident that research objectives are needed to be enriched and further key indices to be included in order to further expand the knowledge in this field. A main research gap that stems from the relevant literature is the limited number of works studying building thermal zones, passive construction elements, HVAC systems, and ADBEs as an undivided system of interacting components. An additional task that previous investigations have not fully resolved is to keep the component modeling as detailed and accurate as possible, by avoiding simplifying assumptions. Moreover, the combination of façade components, such as BIPVs, SAHs, and mechanical ventilation units, was not part of the investigation in previous works. Finally, previous studies did not evaluated the overall system performance; instead, the main objective was the estimation of the thermal performance and efficiency of individual components. In this context, the purpose of this paper is to simulate and evaluate the annual performance improvement of two building spaces retrofitted with ADBEs in terms of energy consumption reduction, RES harvesting increase, and indoor thermal quality enhancement. The first building is located in Cardiff, Wales, and its ADBE is equipped with BIPVs, thermal insulation, and an SAH. The second building is located in Grevena, Greece, and its ADBE is equipped with BIPVs, thermal insulation, and a mechanical ventilation system. ADBE designs are graphically presented in Figure 1. It should be noted that these buildings are actual demonstrator sites of the Plug-n-Harvest Horizon 2020 project, the purpose of which is to propose and evaluate sustainable, optimally designed ADBEs for building renovation, given their climate zone, residential structure, and energy requirements. Therefore, the results of this study offer valuable conclusions for the buildings under study and the engaged communities. The simulations are performed using the equation-based, object-oriented Modelica language [20] within the Dymola software environment [21], enabling accurate monitoring of the dynamic evolution of system components' physical quantities and proper capturing of all mutual interactions.
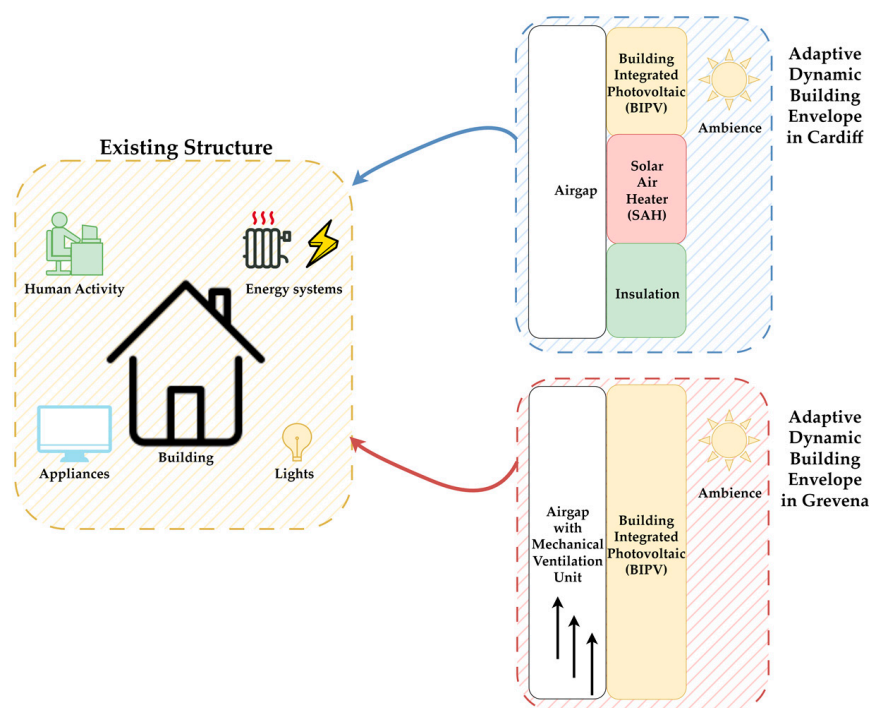

Figure 1. Graphical representation of both ADBE designs under study.

The main contributions of this research are:

- Mathematical modeling of ADBEs as part of broader building systems, involving novel technologies, such as BIPVs, SAHs, and mechanical ventilation units.
- Evaluation of the effect of the installed façades on the sites under study, namely a 60% and a 22% RES share in heating and electricity load coverage for the Cardiff space, respectively, and a 43% share in electricity load coverage for the Grevena space.

2. Materials and Methods

Dynamic building-level simulations have been conducted for the former and latter states of both building spaces under investigation, i.e., before and after the installation of the new façades. To model building thermal zones, construction elements, and heat transfer mechanisms at all system points, the open-source Modelica AixLib library [22] has been used. This library focuses on the dynamic modeling of buildings in a bottom-up approach, namely from internal elements, such as wall material layers, to building interaction with the environment. More specifically, the construction element model (i.e., wall, slab, roof, window, etc.) consists of a number of sequential models of heat conductors and capacitors equal to the number of material layers. Each pair of heat elements retrieves the thermal and geometric properties of the corresponding material layer it represents. The heat transfer mechanisms of each construction element include conduction, convection, and radiation. It should be highlighted that the high-order AixLib model has been selected over the reduced-order to ensure that accuracy is not compromised. The thermal zone model also consists of an air volume model exchanging heat and mass flows with its adjacent construction elements and the environment, being able to operate as a heat source/sink for the building, depending on the weather/indoor conditions, the heat gains from available solar radiation, and internal activity.

Certain component models, which play an important role in energy consumption/savings and system efficiency, needed development from scratch or certain customizations. In this respect, their mathematical models, used for simulations, are described in detail below.

2.1. Solar Air Heater

The Solar Air Heater (SAH) is an active component that can be mounted on a building façade and transfers collected heat, provided by solar radiation, into the room. Except for the provision of heat, the SAH can also ensure room ventilation, since it is an open-loop component that uses ambient air as its working medium. As an active component, the air circulation is caused by an attached fan, which, depending on the commercial SAH model, can be powered by a low-power photovoltaic cell or directly by the grid. SAHs are available in many different types and sizes, depending on the manufacturer and model.

The operation of the SAH considered in this study is as follows. An ambient airflow enters the SAH. Solar radiation penetrates the cover and is absorbed by the absorber. The airflow temperature increases mainly by the heat received from the absorber through convection. Finally, the heated airflow is injected into the building interior.

The main technical characteristics of the SAH, as provided by the manufacturer, are given in Table 1.

Table 1. Technical characteristics of the Solar Air Heater (SAH).

Quantity	Value
Length (mm)	2000
Width (mm)	1006
Nominal air volume flow rate (m^3/h)	125

According to assumptions, the technical characteristics of the SAH, used for the simulations can be seen in Table 2.

Table 2. Assumptions about the technical characteristics of the SAH.

Quantity	Value
Cover transmittance coefficient	0.7
Cover U-value (W/(m²·K))	3.0
Absorber length (mm)	1800
Absorber width (mm)	905.4
Absorber thickness (mm)	2
Absorber density (kg/m³)	1200
Absorber specific heat capacity (J/(kg·K))	1200

The absorber volume is calculated as:

$$V_{abs} = L_{abs} \cdot W_{abs} \cdot D_{abs} \tag{1}$$

where L_{abs}, W_{abs}, and D_{abs} are the absorber's length, width, and depth, respectively (in m). The absorber heat capacity, C_{abs} (in J/K), is given by:

$$C_{abs} = \rho_{abs} \cdot c_{abs} \cdot V_{abs} \tag{2}$$

where ρ_{abs} is the density (in kg/m³), c_{abs} is the specific heat capacity (in J/kg/K), and V_{abs} is the volume (m³) of the absorber.

Finally, based on the manufacturer datasheet, with 1000 W/m² radiation, the air volume flow rate can reach up to its maximum value of 125 m³/h to provide the peak thermal power output (1.4 kW$_p$). The model developed for the SAH is presented in Figure 2 (Dymola environment). To model the air passages of the flow entering and leaving the collector, two pipes have been considered, while the heat transfer mechanisms between the flow and the absorber have also been taken into consideration. Furthermore, operation control actions are implemented in order for the space temperature setpoint to be respected and the inlet stream temperature always to exceed room temperature, or equivalently, allow the component to operate solely as a heat source.
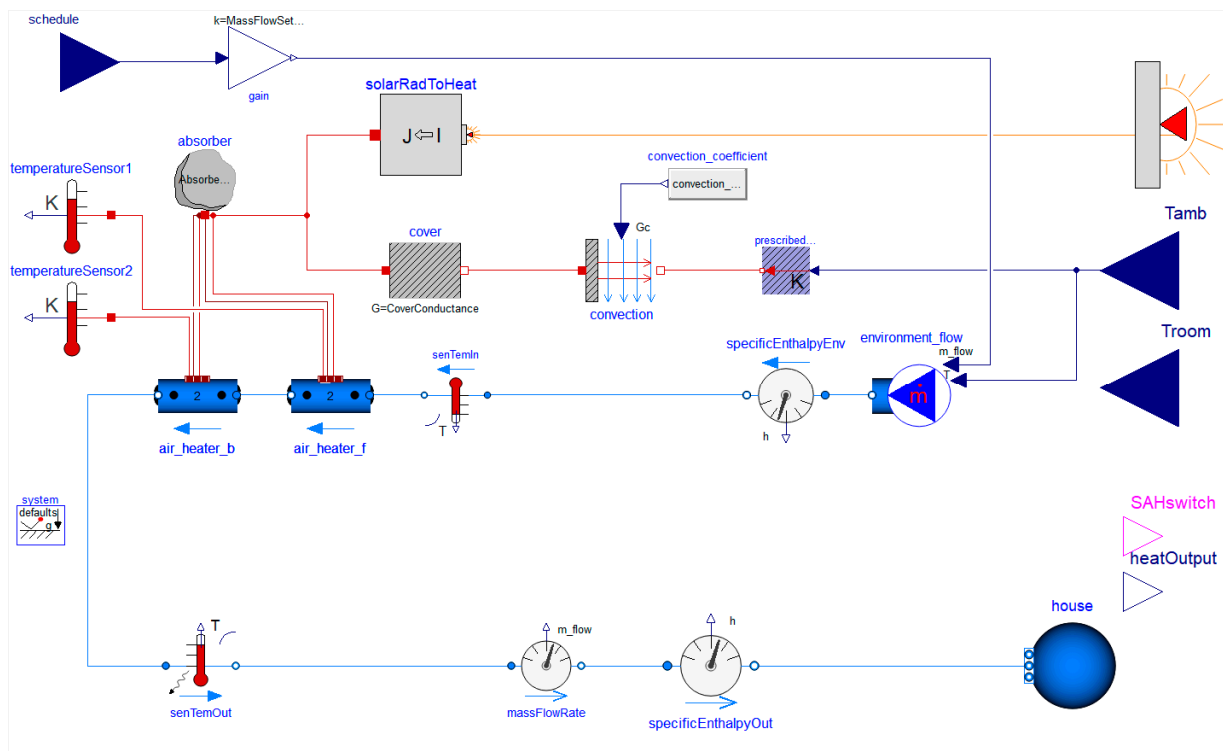

Figure 2. Graphical representation of the SAH model developed within the Dymola environment.

2.2. Gap Ventilation

Due to the installation of a new façade in front of the already existing walls, there is a narrow air gap between the two types of surfaces. This gap is important from two main aspects: (a) the low air gap flow acts as an additional insulation layer, especially for the cold periods of the year and (b) the cooling effect of the gap's air flow on the PV panel improves its efficiency. In this study, the focus is given to the first aspect to capture the effects of the air gap on the building's thermal behavior. However, according to [17], the technology implemented for PV ventilation (natural, mechanical, and no ventilation) may lead to a maximum variability of 0.7% in its electricity generation, even in hot tropical climate conditions. Therefore, the accuracy of the PV production estimation is slightly affected by this assumption. In this regard, the mathematical model of the air gap consists of an air volume that is connected with the infiltration ports of ambient air and the existing wall mass transfer ports. In this way, the infiltration mechanism of the room is modelled by the air gap model by directly linking the environment with the wall's ports. Therefore, the infiltration air flow through the air gap is assumed to be unaffected by the thermal interaction with the adjacent surfaces (façade, existing wall). However, the component of air volume is assumed to be full of motionless air that increases its temperature through the exchanged heat, thus acting as an additional insulation layer to the building, especially for the cold periods of the year.

2.3. Mechanical Ventilation Unit

The model developed within the Dymola environment to describe the operation of the mechanical ventilation unit is presented in Figure 3. The main operation of this component is to provide the room with fresh, ambient air to enhance the interior conditions for the occupants. Furthermore, the recuperator brings the inlet stream temperature closer to the interior one. More specifically, the unit sucks air from the outside atmosphere and passes it through a recuperator in order for its temperature to be brought closer to the building's interior temperature. In this framework, when the ventilation unit is turned on by the users, the mathematical model considers a fan unit sucking air from outside and a second fan unit sucking air from the room through two respective port connections, while the heat exchange between the two streams is implemented through a suitable counter-flow heat exchanger model with 90% effectiveness.
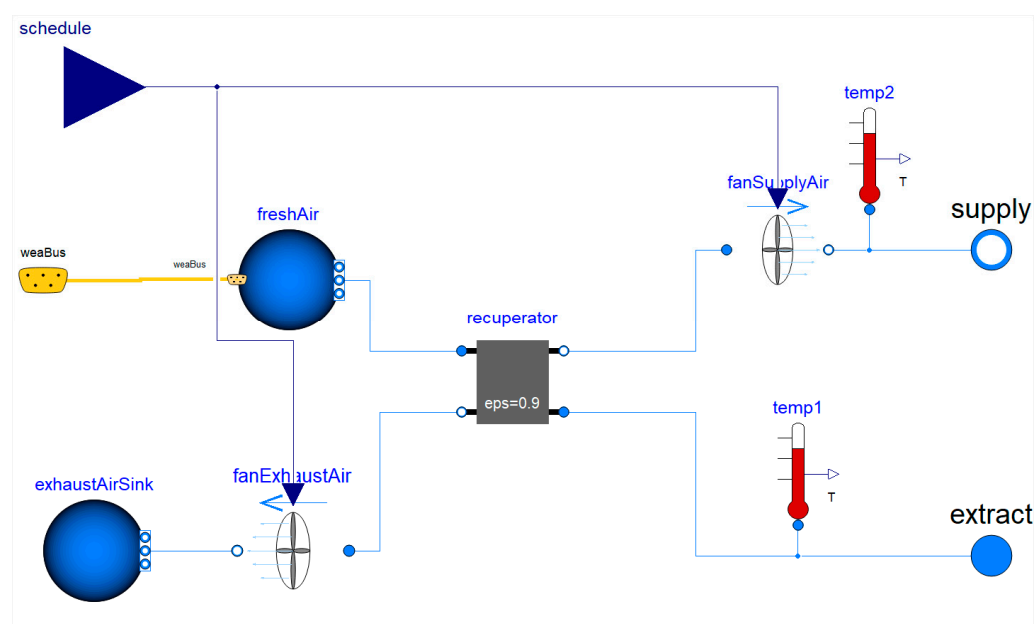

Figure 3. Graphical representation of the mechanical ventilation unit developed within the Dymola environment.

2.4. BIPV Module

For the simulation of the building-integrated PVs (BIPVs) on top of the installed façades, the model developed by the AixLib library has been utilized. The following widely accepted equation set is used, as proposed by [23,24]:

$$T_c = T_a + \frac{G_T}{G_{NOCT}} \cdot \left(T_{c,NOCT} - T_{a,NOCT} \right) \tag{3}$$

$$P_{PV} = P_{PV,STC} \cdot \frac{G_T}{G_{STC}} \cdot \left(1 - \gamma \cdot (T_c - T_{STC}) \right) \tag{4}$$

where T_c is the PV cell temperature (in $^{\circ}$C), T_a is the ambient temperature (in $^{\circ}$C), G_T is the measured solar radiation intensity (in W/m^2), $T_{c,NOCT}$ is the nominal operating cell temperature (NOCT) (in $^{\circ}$C), G_{NOCT} is the solar radiation intensity at which the NOCT is defined (in $^{\circ}$C), $T_{a,NOCT}$ is the ambient temperature at which the NOCT is defined (in $^{\circ}$C), P_{PV} is the cell output power (in W), $P_{PV,STC}$ is the cell output power in Standard Test Conditions (STC) (in W), G_{STC} is the solar radiation intensity at STC (in W/m^2), γ is the cell output power temperature coefficient (in $^{\circ}$C^{-1}), and T_{STC} is the standard measurement temperature (in $^{\circ}$C).

In the cases studied in this work, three different types of PVs were examined. Their specifications, as provided by the manufacturers, are listed in Table 3.

Table 3. Technical specifications for the PV modules installed.

	#1	**#2**	**#3**
PV type	PV	PV	PV window
Location	Grevena	Cardiff	Cardiff
Installed capacity	6 kW	166 W	86 W
Efficiency	5.3%	15.74%	2.81%
Total PV area	38 m^2	1.05 m^2	3.05 m^2
Cell output power temperature coefficient	0.0043 $^{\circ}$C^{-1}	0.0038 $^{\circ}$C^{-1}	0.0019 $^{\circ}$C^{-1}
Nominal operating cell temperature		46 $^{\circ}$C	
Standard measurement temperature		25 $^{\circ}$C	

2.5. Load Scheduling, Internal Heat Gains, and Weather Data

The equipment and the users of a room are both considered to contribute to its heating. For this purpose, internal heat gains are also considered. In particular, the machinery heat gains are modeled with the use of DIN V 18599, depending on the zone type, and their emissivity is considered to be equal to 0.90. Furthermore, the lighting heat gains are also modeled according to DIN V 18599, where the illuminance is calculated based on the type of zone, and their emissivity is considered to be equal to 0.98. In addition, the heat output of the occupants inside the room, whenever they are present, is modeled according to VDI 2078. Finally, typical meteorological year (TMY) weather datasets of the time interval 1983–1995 have been used for the simulations. For the estimation of the available solar irradiance, the transposition model of Perez [25] has been used. Transposition is the calculation of the incident irradiance on a tilted plane using the horizontal irradiance data.

3. Use Cases

3.1. Demonstrator Site in Cardiff, Wales

The Welsh demonstrator site is located in Cardiff and is represented by a room on the ground floor of an office building, which is currently being used as a storage space. Based on the Köppen classification, Cardiff belongs to the Cfb climate group, namely temperate oceanic climate or subtropical highland climate with no dry season and warm summer. Maximum and minimum monthly temperatures average 21.8 $^{\circ}$C (July) and 2.47 $^{\circ}$C (February). After proper radiation transformations, the maximum monthly available solar irradiance on the vertical surface varies from 483 W/m^2 (December) to 805 W/m^2 (March).

The selection of this location is based on the need to prove the applicability of the proposed system in an area with mainly mild weather, often cloudy, wet, and windy. Subsequently, the climate conditions render this pilot site ideal for examining the system performance in a region with low average daily sun hours. The façade is installed on the southeast wall of the room.

In the current version of the building, the appliances used in the examined room include a lighting system of three fluorescent tubes of a nominal power of 70 W each. The lighting system is expected to remain the same after the renovation of the building. Furthermore, in order to cover the space heating requirements during the winter period, the room is heated through the central heating system, powered by a natural gas boiler. At both states, i.e., before and after the façade implementation, the heating system was modeled through a radiator of 1 kW nominal capacity and 90% efficiency. The operation of the terminal units is expected to be controlled by a thermostat in respect of the ideal room temperature range, i.e., between 21 °C and 23 °C during winter.

The proposed façade for the Welsh pilot will be installed on top of the existing southeast wall at a distance of 85 mm (the width of the air gap) and consists of specially designed aluminum frames for the support of the integrated PV panels and the SAH. Installation of the PV system aims to provide electricity to the room and incorporates two types of panels: (a) one opaque panel, and (b) two semi-transparent panels (PV windows) on top of the existing windows (for their technical characteristics see Table 3). The SAH installation is necessary to provide auxiliary heating through renewable sources and not conventional fuels. In this study, SAH was considered to be installed on the right side of the façade covering an area of approximately 2 m^2 with a maximum thermal power output of 1.4 kW$_{th}$. The construction of the whole façade and its subcomponents can be seen in Figure 4. In addition, the inner walls and ceiling of the room were all considered adiabatic surfaces since they are adjacent to heated thermal zones. Due to the lack of information about soil thermal properties, an adiabatic boundary condition between the slab surface and the ground has been considered. According to [26], the error caused by this simplification in indoor temperature calculation is acceptable. Their construction materials are also presented in Figure 4, while the respective physical properties, not provided by the manufacturers, are defined by [27]. Regarding the windows, the thermal transmittance and the coefficient of the solar energy transmission were considered to be equal to 2.665 W/(m^2·K) and 0.703, respectively. Additionally, based on the manufacturer, the respective parameters for the semi-transparent PV windows of amorphous silicon in front of the existing building's windows were defined as equal to 1 W/(m^2·K) and 0.15, respectively.
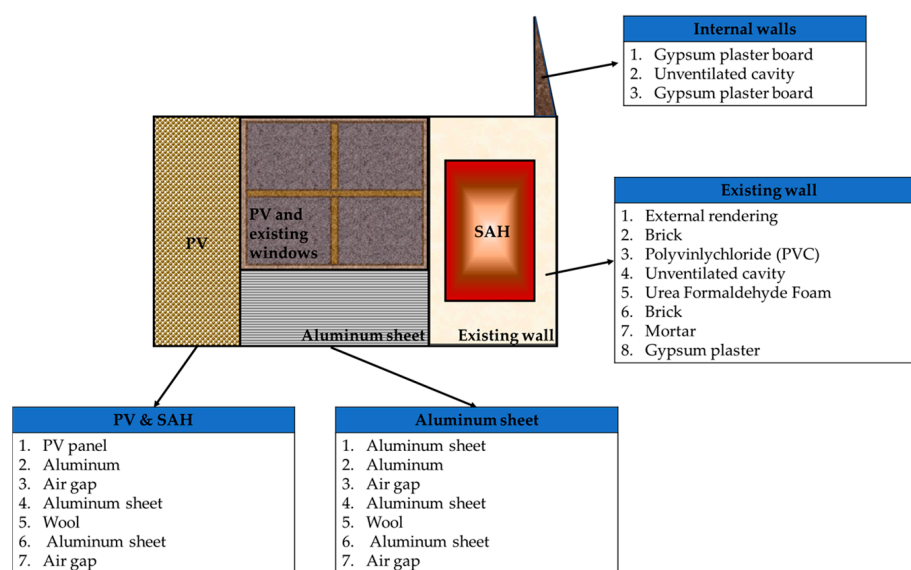

Figure 4. Formation of the Welsh ADBE system.

Finally, the room's ventilation was based on passive means, such as natural ventilation through the window and infiltration through the walls. Since there is no information or experimental data, a series of assumptions have been made. More specifically, the total air change rate can be set either to 0.6 cycles per hour (h^{-1}) due to infiltration or to 3 h^{-1} due to opening of the window, when the room temperature exceeds 25 °C [28,29] during both working and non-working hours. As the work schedule, Monday through Friday from 9 a.m. to 5 p.m. has been considered.

3.2. Demonstrator Site in Grevena, Greece

The Greek demonstrator site is located in Grevena, a northwestern city of Greece in the Region of Western Macedonia (RWM). It is a public building that hosts municipal authorities. Based on the Köppen classification, Grevena belongs to the Csb climate group, namely the warm-summer Mediterranean climate. Maximum and minimum monthly temperatures average 29.6 °C (July) and −1.2 °C (January). After proper radiation transformations, the maximum monthly available solar irradiance on the vertical surface varies from 435 W/m^2 (June) to 896 W/m^2 (February). Consequently, this large difference in temperatures exhibited between winter and summer renders this demonstrator ideal for examining the system's performance in a wide range of temperature conditions. In this case, the ADBE is installed on the southeast corner of the building, including two rooms (one room per floor); however, in this study, only one floor and, therefore, one room was considered.

The proposed façade for the Greek pilot site will be installed on top of the existing wall at a distance of 300 mm (the width of the air gap) and consists of assemblable aluminum frames for the support of the utilized PV panels and the mechanical ventilation unit. Their construction materials are presented in Figure 5, while their physical properties are defined by the constructor. The frames in front of the walls will also be equipped with a 30 mm insulation layer (0.036 W/(m·K) thermal conductivity) in order to minimize the thermal losses to the ambient air. The installed PV panels are of two types: (a) opaque fixed panels, which are expected to be installed in front of the building's walls, and (b) semi-transparent PV windows of amorphous silicon in front of the existing building's windows. The nominal power per unit surface of the selected opaque fixed panels and semi-transparent PV windows are 57.6 W_p/m^2 and 34 W_p/m^2, respectively. Using a weighted arithmetic mean based on the ratio of the PV surfaces, the efficiency is supposed to be equal to 5.3%, regardless of the type of the installed PV. The thermal transmittance and the coefficient of the solar energy transmission of the existing windows of the room are estimated to be equal to 2.6 W/(m^2·K) and 0.60, respectively. In addition, based on the manufacturer, the respective parameters for the semi-transparent PV windows of amorphous silicon in front of the existing building's windows are defined as equal to 5.7 W/(m^2·K) and 0.34, correspondingly.
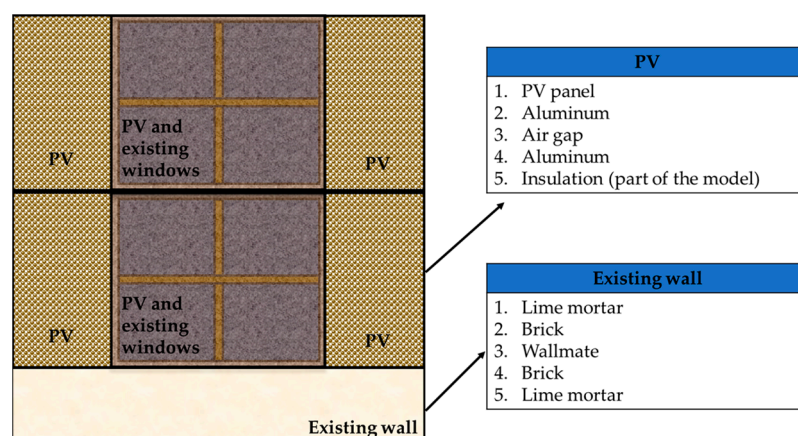

Figure 5. Formation of the Greek ADBE system.

The mechanical ventilation unit's operation is approximated by assuming two operation modes: the first, when occupants are absent, is defined by an inlet volume flow rate of 33 m³/h (0.011 kg/s), and the second, when occupants are present, by an inlet volume flow rate of 51 m³/h (0.017 kg/s). These values correspond to 0.30 h^{-1} and 0.46 h^{-1} air exchange rates for the low and high operation modes, respectively. It should be noted that in the former state of the building under investigation, there was no mechanical system for providing the necessary air exchange, so this process is based on mainly wind-driven ventilation through open windows and infiltration with a total air change rate equal to four cycles per hour throughout the year, both for working and non-working hours [28].

In order to further set up the mathematical model, it is necessary to define the heat gains by the presence of humans and the operation of appliances and systems for both states of the investigated building, i.e., before and after the retrofitting actions. The profile of the human activity inside the room remains unchanged between the cases and foresees 2–3 occupants in the time interval between 7:00 a.m. and 4:00 p.m. from Monday to Friday and no occupants during the weekend since the investigated rooms are offices of the public sector.

In the former state of the building, the appliances used in the examined room included: (a) three personal computers and monitors with a nominal power of 300 W each, (b) two printers/scanners with a nominal power of 150 W each, and (c) two fridges with a nominal power of 90 W each. The utilized appliances were not subject to changes after the renovation of the building. On the contrary, the lighting system was upgraded to a new lighting system for better visual comfort, i.e., an environment with the required quantity and quality of light.

The room is heated through the central heating system, powered by an oil boiler. In order to match the numerical results with the reference value in terms of the thermal energy provided, a radiator with a 2.5 kW nominal capacity was selected. Even though the room was not equipped with a thermostat and the operation of the system is continuous, when the occupants are present the heater is supposed to be controlled by a thermostat. The reference temperature was set to 19.5 °C, thus component actions are performed to maintain the room's temperature near the desired setpoint.

4. Results

4.1. Results of Demonstrator Site in Cardiff, Wales

In this study, the parameters under investigation were the level of the temperature inside the room, indoor thermal quality, the PV generation, the SAH generation, and the electric and thermal demand throughout the year. The temperature inside the room before/after the renovation actions is presented in Figure 6. In the former state of the building, the temperature during the working hours of winter was kept between 21 °C and 23 °C due to thermostat operation. During the night, which is considered an inactive period for the space heating system, significantly lower levels of temperature occurred. The minimum temperature was as low as 6.7 °C. During the rest seasons, both during working and non-working hours, the highest temperature values exceeded 23 °C and this can be explained by the lack of any cooling or/and mechanical ventilation systems and shading devices. The highest temperature exhibited during the summer was equal to 35 °C. After the renovation, the thermostat controls the room temperature, during the winter period and during working hours. During non-working hours, the room still experienced low temperatures, but the local minima were higher than the case before the renovation since the additional insulation installed on the building lowers the heat losses to the environment. During the summer, the room was expected to experience lower temperature maxima (approximately 28.5 °C). The lower temperature peaks can be explained by the installation of the PV windows, the PV panel, and the SAH, which reduce the radiation inserted in the room and the heat absorbed by the room's walls, due to the additional components' lack of or semi-transparency. This leads to a counterbalancing of the overheating phenomenon that takes place owing to the lack of typical shading measures.
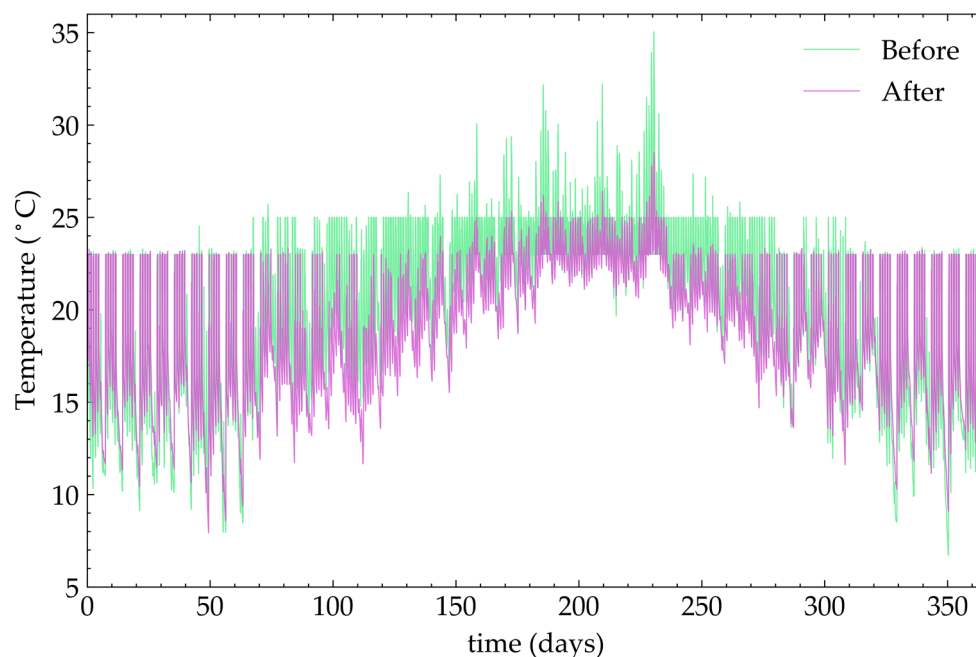
Figure 6. The Welsh pilot room temperature (in °C) before/after the renovation.

The room temperature distribution into classes during working hours throughout the year for both states is presented in Figure 7. It can be assumed that the temperature range for thermal quality is 18–23 °C during winter (21–23 °C is the thermostat setpoint range) and 18–24 °C during summer. Therefore, in order to extract meaningful conclusions, the temperature values have been sorted into three classes: (a) values lower than 18 °C, (b) values between 18 °C and 24 °C, and (c) values higher than 24 °C. A key output of the results is that during 37% of the working hours, before the renovation of the building, there was feelings of discomfort for the occupants due to higher/lower temperatures than the desired temperature range. In comparison with the results before retrofitting, the frequency of discomfort after the renovation actions decreased to 17% for the year. The frequency of the highest temperature values (>24 °C) dropped to 10% from 32% due to the installation of the PV, the PV windows, and the SAH that act as shading devices, while the frequency of the lowest temperatures (<18 °C) was almost unaffected and was in the range of 5–7%. However, a notable differentiation in the results was the increase in operating hours between 18 °C and 21 °C, from 4% to 35%. This can also be explained by the reduction of incoming radiation due to the installation of additional components and semi-transparent PV windows. Even if this increase does not radically affect the occupants' comfort, it can be translated into significant heating demands.

Indeed, as can be seen upon observing Figure 8, which presents the heating load of the room before/after the renovation, from March until October, the thermal needs of the room were increased; the highest differences were experienced in spring. This is directly attributed to the lower radiation into the room due to the additional components installed and the increased required load to maintain the room temperature inside the desired range. However, since the SAH was exploited as an auxiliary heating source after the renovation, the total energy provided by the central heating system was decreased. More specifically, in the prior state of the building, the heating energy demand of the room, which was covered exclusively by the existing central heating system, was estimated at 356.3 kWh. This is equivalently translated into 50 m^3 total natural gas consumption, given that the total efficiency of the heating system was equal to 81% and the natural gas net heating value was as high as 31.7 MJ/m^3 at standard temperature and pressure conditions. After the renovation of the building, the thermal contribution was calculated to be 314.3 kWh and the total natural gas consumption was 44.1 m^3, a reduction of approximately 12%.

Therefore, it is concluded that this decrease in the use of the central heating system was indeed affected by the SAH's contribution.
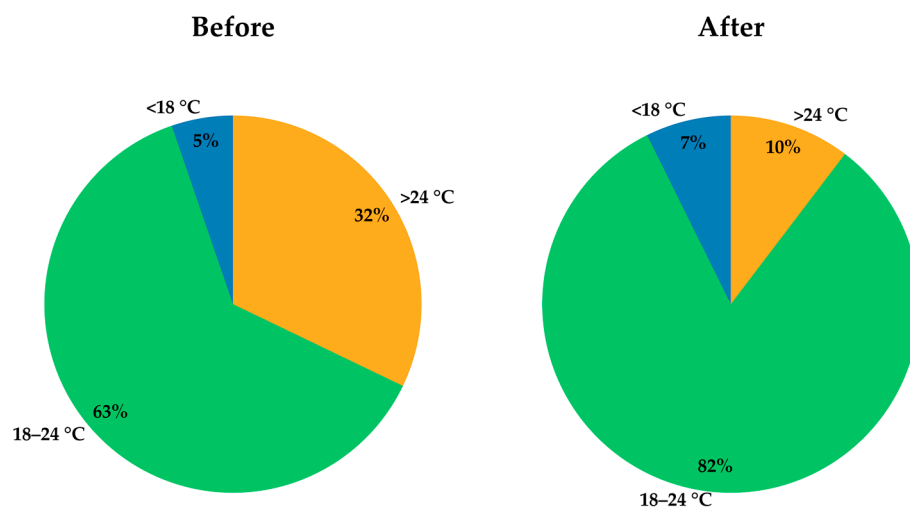
Before

After

Figure 7. Room temperature distribution of the Welsh pilot site while occupants are present in the room before and after renovation.
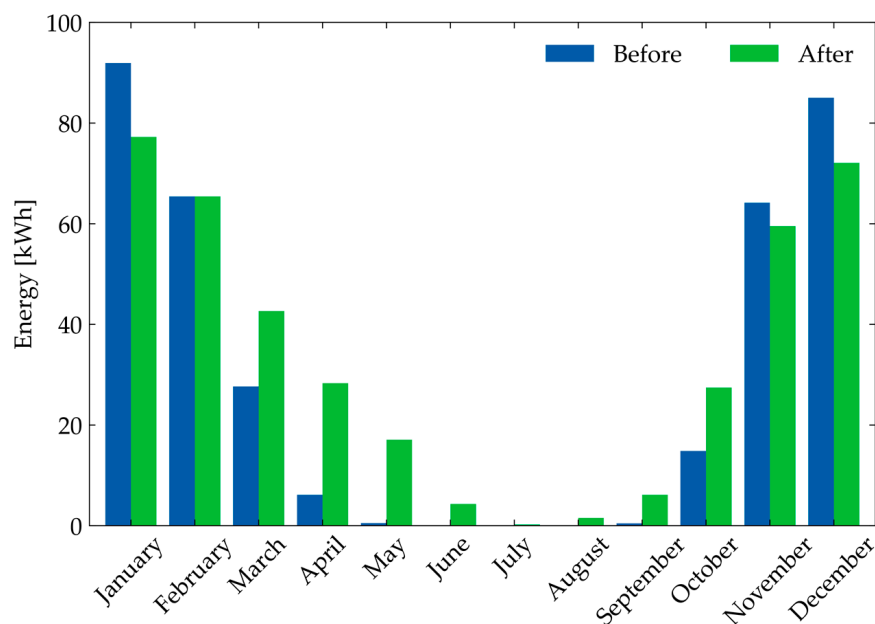
Figure 8. Heating energy load of the Welsh site room before and after the renovation.

At this point, it should be highlighted that in order to properly select SAH specifications for optimized SAH's contribution, a sensitivity analysis was conducted at a preliminary level. Multiple values of air supply volume flow rate, as well as the option to operate during additional hours, even during users' absence, have been examined. Based on the results of this analysis, listed in Table 4, the maximum value of energy contribution was achieved with a volume flow rate equal to 10% of the nominal value (12.5 m^3/h) and additional operation (beyond users' presence schedule) between 7 a.m. and 9 a.m. The control conditions, specified in Section 2, should also be respected. More specifically, the component operates when: (a) its production causes the room temperature not to exceed the upper limit of the desired range in winter (23 °C), and (b) the inlet stream temperature is higher than the room temperature.

Table 4. Sensitivity analysis on the effect of air volume flow rate and operating hours on SAH energy contribution.

Case	Operating Condition	Annual Energy Contribution from SAH (kWh)	Annual Energy Contribution from the Existing Heating System (kWh)
1	(a) 50% of the nominal air volume flow rate	44.3	400.0
2	(a) 50% of the nominal air volume flow rate (b) additionally on from 7 a.m. to 9 a.m.	48.7	401.7
3	(a) 30% of the nominal air volume flow rate (b) additionally on from 7 a.m. to 9 a.m.	71.6	364.2
4	(a) 10% of the nominal air volume flow rate (b) additionally on from 7 a.m. to 9 a.m.	87.7	314.3

Based on the above process, the SAH production was estimated as 87.7 kWh in total, which is 21.8% of the annual heating load. Based on Figure 9, the contribution of SAH to the total heating load of the room per month showed a vast range, i.e., from below 10% to 100%. The highest percentages were experienced during the summer period, when the thermal needs concern individual days with very limited thermal loads. During the winter, the SAH contribution showed the lowest values (approximately 10%) due to the very low available radiation and temperature levels experienced in the region, which affected the efficiency of the system and its capability to operate as a heat source.
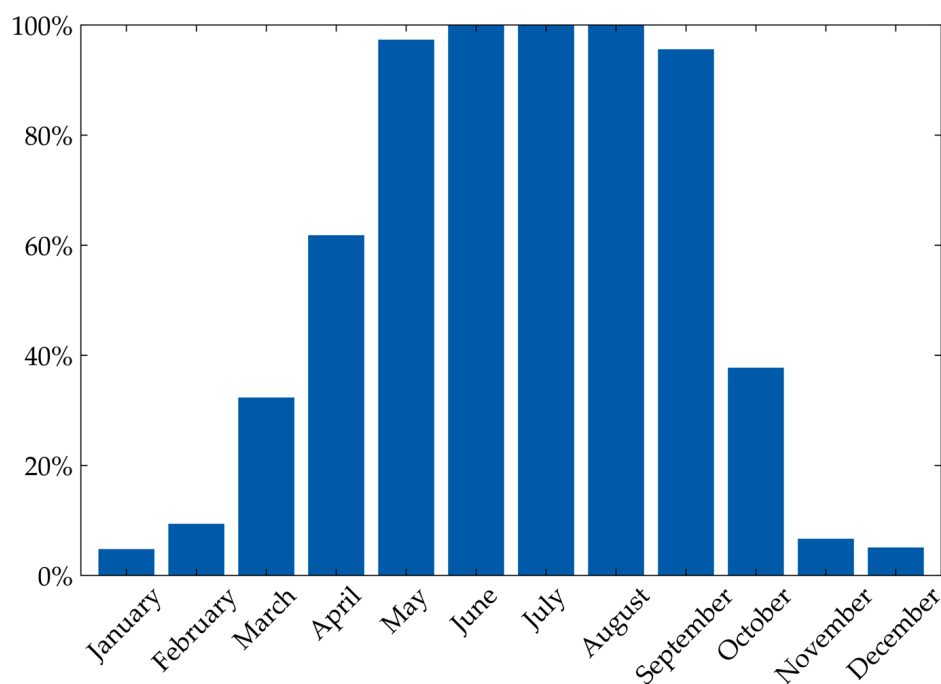
Figure 9. SAH contribution percentage throughout the year after the renovation of the Welsh site room.

Nevertheless, based on the results, the thermal demand in the post-retrofit state of the building, covered by both the SAH and boiler, seemed to be higher than the respective value in the current state of the building, i.e., 402 kWh against 356.3 kWh, which is equivalent to a 13% increase. This, as already explained, is attributed to the effect of structure and components that were installed after the retrofit actions.

According to the simulations, the PVs resulted in an annual electrical energy generation of 239.9 kWh (60% of the annual load of the room) with a maximum power of approximately 210 W, i.e., 83.3% of the installed capacity. The monthly PV percentage contribution to the room's load is shown in Figure 10. According to this, even during the coldest period of the year (October–March), the PV load coverage ranges between 25 and

75%, thus paving the way towards the enhanced autonomy of the building from the grid, even during the days with low solar radiation.
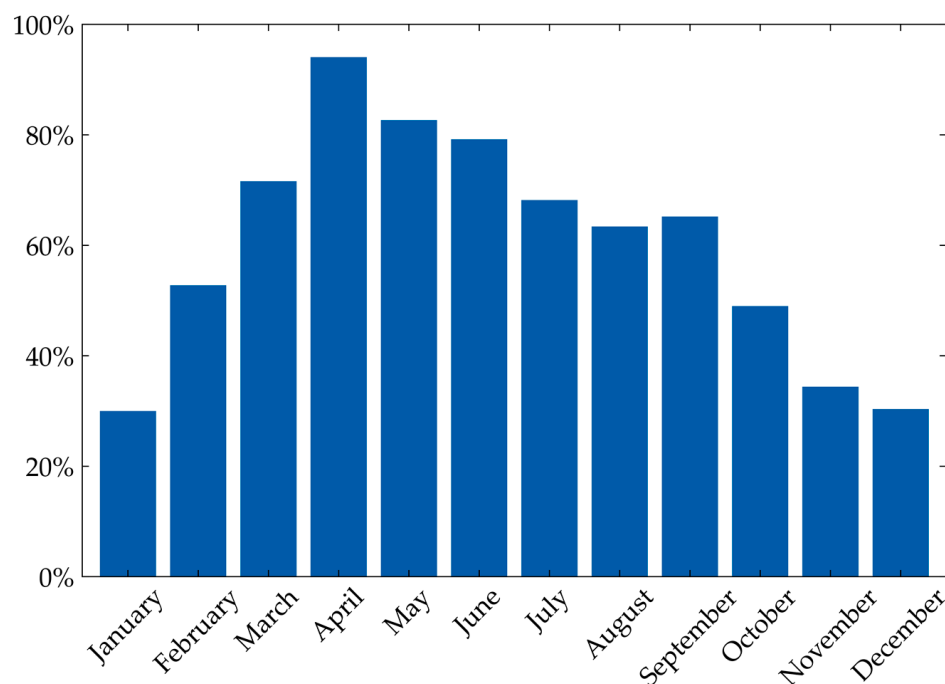

Figure 10. PV electricity load coverage per month after the renovation of the Welsh site room.

In Table 5 the simulation results regarding the electric and thermal energy demand of the room before and after the installation of the façade are summarized. A significant amount of electrical energy, namely 60% of the required load, was produced by the PV systems. A notable result was the decrease of the annual natural gas consumption by approximately 12%, even if the annual thermal demand was slightly increased by 13%, due to the contribution of the SAH component. The increase in thermal demand, as already noted, can be explained by the shading effect caused by the components installed and the resulting decrease in the radiation entering the room. Therefore, although these mechanisms provide protection from overheating during the summer months, they cause a reduction of the solar gains during winter and, thus, lead to a slightly increased energy consumption for space heating.

Table 5. Annual energy outputs before and after the installation of the Welsh site façade.

Quantity	Before Renovation	After Renovation
Electrical energy consumption (kWh)	400.2	400.2
PV production (kWh)	-	239.9
Total thermal energy demand (kWh)	356.3	402.0
Thermal energy provided by the main heating system (kWh)	356.3	314.3
Thermal energy provided by the SAH (kWh)	-	87.7
Natural gas consumption (m^3)	50	44.1

4.2. Results of Demonstrator Building in Grevena, Greece

This subsection is dedicated to the simulation results of the demonstrator building in Grevena, Greece. In Figure 11, the temperature inside the room before/after the renovation actions is presented. In both cases, it was noted that in the presence of occupants during the winter the temperature is regulated at 19.5 °C by the thermostat/heater in order to ensure the desired thermal conditions. Additionally, the interior temperature of the room

during summer, when occupants are present, and especially at noon, reached very high values, higher than 30 °C. This can be attributed to the high ambient temperature levels of the region, the lack of a cooling system, and the absence of solar shading. However, in the post-retrofit state of the building, the highest temperature values were slightly decreased, due to the installation of the façade and its PV windows, both of which decreased the solar radiation entering the room or preventing it from reaching the existing wall. Finally, in both states of the building, while the occupants are absent, the heater was deactivated, causing the room temperature to follow the trend of the ambient temperature.
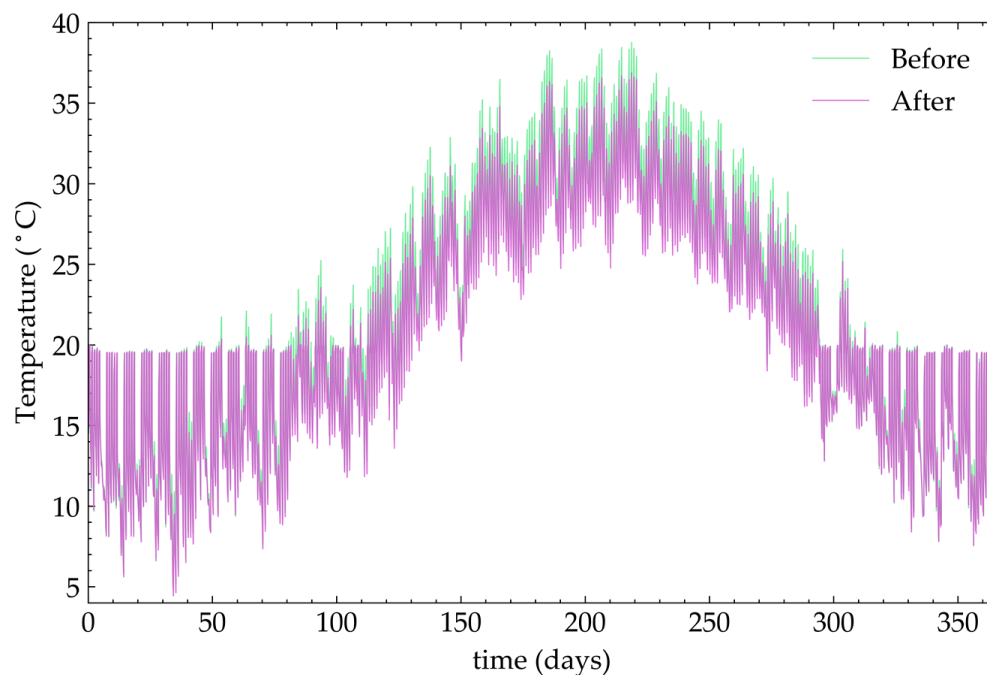

Figure 11. The Greek pilot room temperature (in °C) before/after the renovation.

Figure 12 presents room temperature distribution in classes during working hours throughout the year for both states. Again, in order to extract meaningful conclusions, the temperature values have been sorted into three classes: (a) values lower than 18 °C, (b) values between 18 °C and 24 °C, and (c) values higher than 24 °C. It was noted that after the renovation actions, while occupants are inside the room, the temperatures were slightly shifted towards lower values. According to the results, after the renovation, the frequency of temperature values lower than 18 °C was practically unaffected. However, the frequency of the temperature values that were higher than 24 °C slightly decreased from 46% to 43%, denoting a slight improvement in maintaining the indoor temperature within the occupants' desired range. The general trend of the room temperature values towards lower values is attributed to three main factors: (a) the additional insulation of the interior from the ambient conditions owing to the implementation of the façade, which during summer results in lower room temperature values, (b) the operation of the mechanical ventilation unit that provides the room with additional air of lower temperature than the room during the winter, except for the air that is supposed to be inserted through the infiltration mechanism, and (c) the installation of PV windows that reduce the solar radiation entering the room.

The heating load of the room per month, before and after the renovation actions, is presented in Figure 13. According to the results, the heating load was increased throughout the year with the highest absolute increase taking place in two sequential months, namely February and March. Overall, the thermal energy provided by the heater on an annual basis after the installation of the façade was calculated as equal to 1530 kWh, instead of 1389 kWh, meaning that the heating load of the room was increased by 10% compared to the former

state. This increase can be justified mainly by the significant reduction of the solar radiation entering the room and reaching the building's walls, as already thoroughly explained.
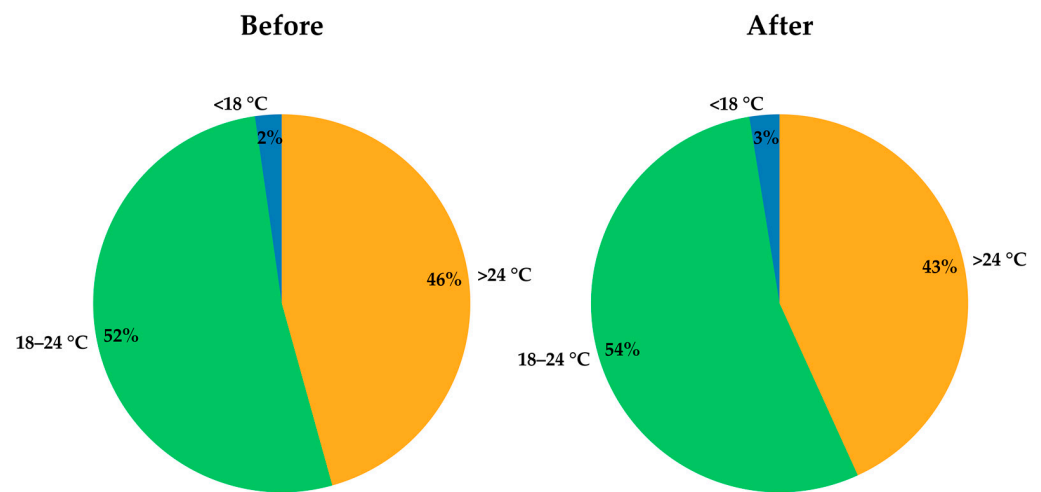

Figure 12. Room temperature distribution of the Greek pilot site while occupants are present in the room before and after renovation.
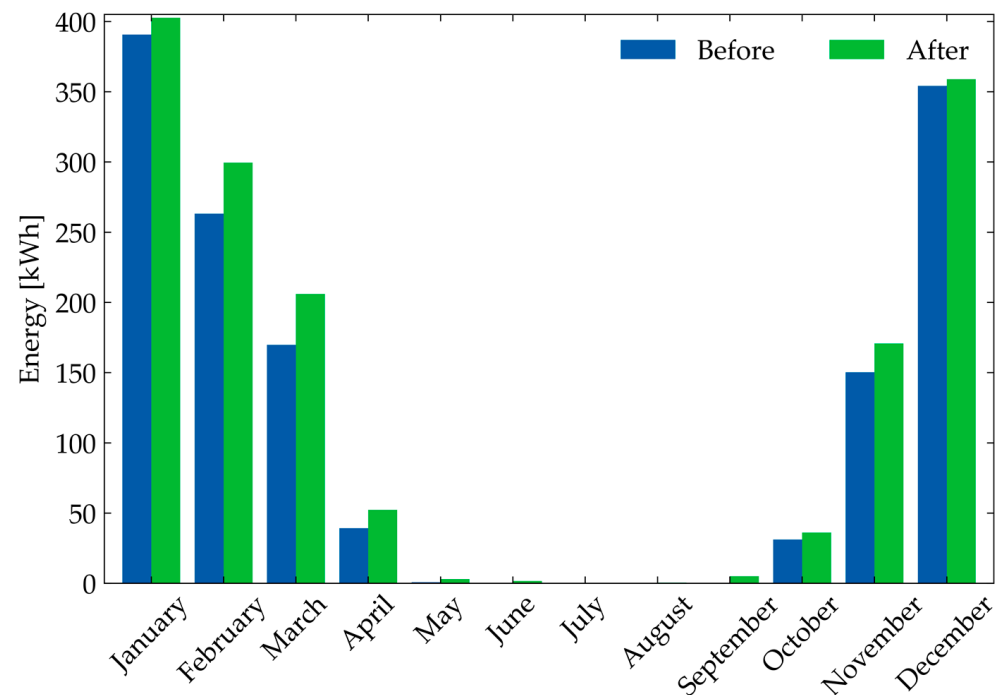

Figure 13. Heating energy load provided to the Greek site room before and after the renovation.

The electrical energy demand was calculated to be increased from 4972 kWh to 5321 kWh annually because of the renovation of the building and specifically the replacement of the lighting equipment. According to the simulations, the installation of the PVs resulted in an annual electrical energy generation of 2277 kWh (42.8% of the annual load after the retrofit). The monthly PV percentage contribution to the room's load is shown in Figure 14. According to this, even during the heating period of the year (October–April), the PV load coverage ranged between 25 and 55%, thus paving the way towards the enhanced autonomy of the building from the grid even during days with low solar radiation.
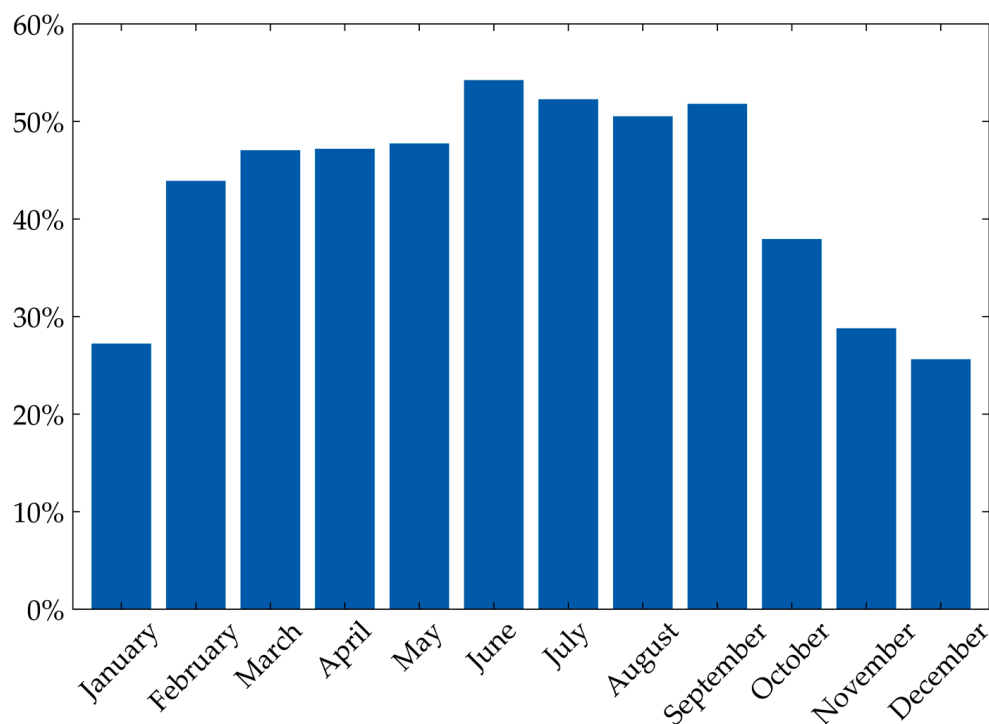
Figure 14. PV electricity load coverage per month after the renovation of the room.

In Table 6 the simulation results regarding the electric and thermal energy needs of the room before and after the installation of the ADBE façade are summarized. The electrical energy provided by the grid after the installation of the sophisticated façade decreased by 39%, from 4972 kWh to 3044 kWh. As regards to the required thermal output of the heater to maintain the indoor thermal quality during the heating period, it was estimated that it will present a slight increase (approximately 10%) due to the reduction of the incoming absorbed solar radiation, owing to the PV components installed on the building. However, the significant reduction of the electrical energy demand due to the installation of the PV panels, the improvement of thermal quality during summer, and the insignificant increase in the thermal needs renders the implemented technology a major energy-efficient building solution.

Table 6. Annual energy outputs before and after the implementation of the installed façade.

Quantity	Before Renovation	After Renovation
Electrical energy consumption by electrical appliances (kWh)	4972	5268
Electrical energy consumption for the mechanical ventilation unit (kWh)	0	53
PV production (kWh)	0	2277
Thermal energy provided by the main heating system (kWh)	1389	1530

Therefore, it is evident from the evaluation of the energetic performance of both pilot sites that the proposed solution is capable of providing enhanced autonomy from the grid, increased RES harvesting, improved interior conditions, and a decrease in conventional fuel consumption. However, the installation of non-transparent or/and semi-transparent modules decreases the radiation entering/affecting the building, so the thermal needs are increased.

5. Conclusions

This research work evaluated the retrofitting option of ADBE façade installations from an energetic point of view using suitable mathematical models. For this purpose, two pilot sites were examined; Cardiff, Wales, and Grevena, Greece. The actual demonstration in two locations with different climates can provide conclusions about the system's operability and

efficiency in a vast range of operating conditions. Furthermore, the inclusion of promising ADBE components, such as BIPVs, SAHs, and mechanical ventilation units, provides the possibility for valuable quantitative evaluation of the contribution of these technologies on the improvement of building performance.

Based on the results for the Cardiff pilot site, the proposed solution was capable of providing an almost 60% share in annual electrical load through PV generation. Regards the interior conditions, the ratio of hours with discomfort for the occupants to the total hours of user presence was been limited from 37% to 17%. Moreover, the SAH unit was estimated to contribute to the annual space heating load by 22%, leading to a 12% decrease in fuel consumption. However, the SAH's share in heating load coverage reduced below 10% during months with extremely low available radiation and temperature levels, namely from November to February. Another finding is that PV and SAH components on the installed façade acted as shading devices leading to a 13% increase in thermal needs.

Regarding the Grevena pilot site, simulation results indicate that the BIPV panels are able to provide an almost 43% share of the annual electrical load. In addition, the ratio of hours with discomfort for the occupants to the total hours of user presence was slightly reduced from 48% to 46%. Finally, the shading effect of the installed components led to a 10% increase in thermal needs, almost the same as in the Cardiff case.

In conclusion, the developed mathematical model focuses on the accurate representation of the ADBE components as interconnected physical entities and the conduction of detailed, dynamic analysis of the whole system in terms of energy consumption, RES harvesting, and indoor conditions. This approach is substantially different from previous studies and methodologies, where the performance and behavior of the ADBE components were studied independently. As a consequence, this work lays the foundations for further investigation of such ADBE solutions, considering them as structures of undivided, continuously interacting components. Due to this specific approach, it is possible to parametrically investigate additional scenarios, considering a different combination of technical components and elements, in order to attain sufficient improvement of the proposed solution. Until now, the research has been focused on the optimization of an individual entity or component that is possible to constitute a part of the whole ADBE construction. On the contrary, this specific investigation is capable of providing designers, possible stakeholders, and other entities with sufficient data for further evaluation of the efficiency, profitability, and sustainability of such retrofitting options as an integrated system.

However, this study also possesses methodological limitations and assumptions that could be addressed by future research work. These simplifications include the consideration of adiabatic interior surfaces, the ideal conditions in terms of human presence and interaction with the building components, the neglect of shading from adjacent buildings, and the limited area of retrofitting. The inclusion of all these aspects in future works is expected to further deepen the understanding of the system's behavior in real operating conditions and provide even more accurate input for the further techno-economic analysis of the retrofit option. This would enable the possibility to enrich the extracted conclusions on how solar-powered ADBE technologies can enhance building energy performance, both during heating and cooling periods.

Author Contributions: Conceptualization, R.R., M.F. and P.D.; methodology, R.R., M.F. and P.D.; software, R.R., M.F. and P.D.; writing—original draft preparation, R.R., M.F., P.D., D.R. and N.N.; writing—review and editing, R.R., M.F., P.D., D.R. and N.N.; visualization, R.R., M.F. and P.D.; supervision, D.R. and N.N. All authors have read and agreed to the published version of the manuscript.

Data Availability Statement: Not applicable.

Conflicts of Interest: The authors declare no conflict of interest.

Nomenclature

ANN	Artificial Neural Network
BIPVs	Building Integrated Photovoltaics
BIPV/T	Building-Integrated Photovoltaic/Thermal
DHW	Domestic Hot Water
DSFs	Double-Skin Façades
EU	European Union
PCMs	Phase Change Materials
PVT	Photovoltaic–Thermal
PVs	Photovoltaics
RES	Renewable Energy Sources
SAHs	Solar Air Heaters
TMY	Typical Meteorological Year
WTs	Wind Turbines

References

1. IEA. Buildings Sectorial Overview. Available online: https://www.iea.org/reports/buildings (accessed on 11 January 2023).
2. Margaritis, N.; Rakopoulos, D.; Mylona, E.; Grammelis, P. Introduction of Renewable Energy Sources in the District Heating System of Greece. *Int. J. Sustain. Energy Plan. Manag.* **2015**, *4*, 43–56. [CrossRef]
3. Mohtashami, N.; Fuchs, N.; Fotopoulou, M.; Drosatos, P.; Streblow, R.; Osterhage, T.; Müller, D. State of the Art of Technologies in Adaptive Dynamic Building Envelopes (ADBEs). *Energies* **2022**, *15*, 829. [CrossRef]
4. Kumar Nigam, P.; Akhtar, S. Retrofitting Practices in Various Categories of RCC Structures—A Comprehensive Review. *Mater. Today Proc.* **2021**, *45*, 7123–7131. [CrossRef]
5. O'Grady, T.; Chong, H.-Y.; Morrison, G.M. A Systematic Review and Meta-Analysis of Building Automation Systems. *Build. Environ.* **2021**, *195*, 107770. [CrossRef]
6. Talaei, M.; Mahdavinejad, M.; Zarkesh, A.; Motevali Haghighi, H. A Review on Interaction of Innovative Building Envelope Technologies and Solar Energy Gain. *Energy Procedia* **2017**, *141*, 24–28. [CrossRef]
7. Luo, Y.; Zhang, L.; Bozlar, M.; Liu, Z.; Guo, H.; Meggers, F. Active Building Envelope Systems toward Renewable and Sustainable Energy. *Renew. Sustain. Energy Rev.* **2019**, *104*, 470–491. [CrossRef]
8. Talaei, M.; Mahdavinejad, M.; Azari, R. Thermal and Energy Performance of Algae Bioreactive Façades: A Review. *J. Build. Eng.* **2020**, *28*, 101011. [CrossRef]
9. Biyik, E.; Araz, M.; Hepbasli, A.; Shahrestani, M.; Yao, R.; Shao, L.; Essah, E.; Oliveira, A.C.; del Caño, T.; Rico, E.; et al. A Key Review of Building Integrated Photovoltaic (BIPV) Systems. *Eng. Sci. Technol. Int. J.* **2017**, *20*, 833–858. [CrossRef]
10. Debbarma, M.; Sudhakar, K.; Baredar, P. Comparison of BIPV and BIPVT: A Review. *Resour. Effic. Technol.* **2017**, *3*, 263–271. [CrossRef]
11. Zhang, X.; Lovati, M.; Vigna, I.; Widén, J.; Han, M.; Gal, C.; Feng, T. A Review of Urban Energy Systems at Building Cluster Level Incorporating Renewable-Energy-Source (RES) Envelope Solutions. *Appl. Energy* **2018**, *230*, 1034–1056. [CrossRef]
12. Calise, F.; Cappiello, F.L.; Dentice d'Accadia, M.; Vicidomini, M. Dynamic Modelling and Thermoeconomic Analysis of Micro Wind Turbines and Building Integrated Photovoltaic Panels. *Renew. Energy* **2020**, *160*, 633–652. [CrossRef]
13. Welcome | TRNSYS: Transient System Simulation Tool. Available online: http://www.trnsys.com/ (accessed on 6 July 2021).
14. Kant, K.; Pitchumani, R.; Shukla, A.; Sharma, A. Analysis and Design of Air Ventilated Building Integrated Photovoltaic (BIPV) System Incorporating Phase Change Materials. *Energy Convers. Manag.* **2019**, *196*, 149–164. [CrossRef]
15. COMSOL. Multiphysics®Software-Understand, Predict, and Optimize. Available online: https://www.comsol.com/comsol-multiphysics (accessed on 9 February 2023).
16. Mei, L.; Infield, D.; Eicker, U.; Loveday, D.; Fux, V. Cooling Potential of Ventilated PV Façade and Solar Air Heaters Combined with a Desiccant Cooling Machine. *Renew. Energy* **2006**, *31*, 1265–1278. [CrossRef]
17. Yang, S.; Cannavale, A.; Di Carlo, A.; Prasad, D.; Sproul, A.; Fiorito, F. Performance Assessment of BIPV/T Double-Skin Façade for Various Climate Zones in Australia: Effects on Energy Consumption. *Sol. Energy* **2020**, *199*, 377–399. [CrossRef]
18. Alhammadi, N.; Rodriguez-Ubinas, E.; Alzarouni, S.; Alantali, M. Building-Integrated Photovoltaics in Hot Climates: Experimental Study of CIGS and c-Si Modules in BIPV Ventilated Facades. *Energy Convers. Manag.* **2022**, *274*, 116408. [CrossRef]
19. Nguyen, D.C.; Ishikawa, Y. Artificial Neural Network for Predicting Annual Output Energy of Building-Integrated Photovoltaics Based on the 2-Terminal Perovskite/Silicon Tandem Cells under Realistic Conditions. *Energy Rep.* **2022**, *8*, 10819–10832. [CrossRef]
20. Fritzson, P. *Principles of Object-Oriented Modeling and Simulation with Modelica 3.3: A Cyber-Physical Approach*; IEEE: Piscataway, NJ, USA, 2015.
21. Dymola-Dassault Systèmes®. Available online: https://www.3ds.com/products-services/catia/products/dymola/ (accessed on 6 July 2021).

22. Müller, D.; Lauster, M.; Constantin, A.; Fuchs, M.; Remmen, P. AixLib—An Open-Source Modelica Library within the IEA-EBC Annex60 Framework. In Proceedings of the BauSIM2016 Conference, Technische Universität Dresden, Dresden, Germany, 14–16 September 2016.
23. Duffie, J.A.; Beckman, W.A. *Solar Engineering of Thermal Processes*, 4th ed.; Wiley: Hoboken, NJ, USA, 2013; ISBN 978-1-118-41812-3.
24. Osterwald, C.R. Translation of Device Performance Measurements to Reference Conditions. *Sol. Cells* **1986**, *18*, 269–279. [CrossRef]
25. Perez, R.; Ineichen, P.; Seals, R.; Michalsky, J.; Stewart, R. Modeling Daylight Availability and Irradiance Components from Direct and Global Irradiance. *Sol. Energy* **1990**, *44*, 271–289. [CrossRef]
26. Luo, C.; Moghtaderi, B.; Page, A. Effect of Ground Boundary and Initial Conditions on the Thermal Performance of Buildings. *Appl. Therm. Eng.* **2010**, *30*, 2602–2609. [CrossRef]
27. Çengel, Y.A.; Boles, M.A.; Kanoglu, M. *Thermodynamics: An Engineering Approach*, 9th ed.; McGraw-Hill Education: New York, NY, USA, 2019; ISBN 978-1-259-82267-4.
28. Yongming, J.; Duanmu, L.; Liu, Y.; Dong, H. Air Infiltration Rate of Typical Zones of Public Buildings under Natural Conditions. *Sustain. Cities Soc.* **2020**, *61*, 102290. [CrossRef]
29. Howard-Reed, C.; Wallace, L.A.; Ott, W.R. The Effect of Opening Windows on Air Change Rates in Two Homes. *J. Air Waste Manag. Assoc.* **2002**, *52*, 147–159. [CrossRef] [PubMed]